

Mechanistic Insights into the Brønsted Acid-Catalyzed Dehydration of β -D-Glucose to 5-Hydroxymethylfurfural Under Ambient and Subcritical Conditions

Sooraj Kunnikuruva^{*,†,‡} and Nisanth N. Nair^{*,†}

[†]*Department of Chemistry, Indian Institute of Technology Kanpur, Kanpur 208016, India*

[‡]*Current address: Department of Chemistry, Bar-Ilan University, Ramat Gan 5290002,
Israel*

E-mail: soorajk@biu.ac.il; nnair@iitk.ac.in

Phone: +91 (0)512 2596311. Fax: +91-(0)512 2596806

Supporting Information

1 Comparison of density of the glucose solution in ABW and SCW

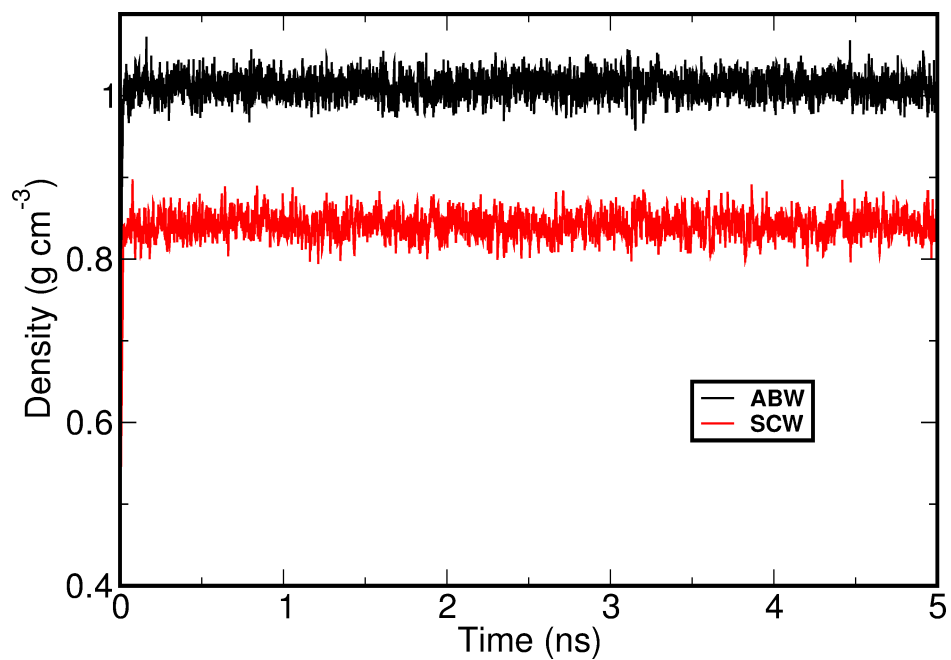


Figure S1: Density of acidified glucose solution in ABW (black curve) and SCW (red curve) plotted against time.

2 Metadynamics parameters

Table S1: Mass of the collective variables (m) and coupling constants (k) used in the extended Lagrangian metadynamics simulations

Collective Coordinate	Label	m (a.m.u.)	k (a.u.)
Distance	d	50.0	2.0
Distance Difference	Δd	50.0	0.5
Coordination Number	C	50.0	2.0
Coordination Number Difference	ΔC	50.0	2.0
Dihedral	ϕ	50.0	0.8

Here, coordination number between atom types A and B is defined as,

$$C = \sum_{I \in A} \sum_{J \in B} \frac{1}{1 + (d_{IJ}/d_{AB}^0)^6} \quad , \quad (\text{S1})$$

where d_{IJ} is the internuclear distance between atom I and J at any point of time, and d_{AB}^0 is the bond distance cut-off parameter. d_{AB}^0 values used in this study between different atom types are given in Table S2.

Table S2: Values of d^0 parameter in Equation (S1) used for different types of atoms during the metadynamics simulation with coordination number collective coordinate

Collective coordinate	d^0 (Å)
$C[\text{C} - \text{H}]$	1.4
$C[\text{C} - \text{H}_{\text{w,OH}}]$	1.3
$C[\text{O} - \text{H}]$	1.3
$C[\text{C} - \text{O}_{\text{w}}]$	1.8
$C[\text{C} - \text{O}_{\text{OH}}]$	2.0

3 List of Collective Variables Used

Table S3: CCs used for modeling various reactions

Reaction	CC	Description	CV Label
G → F1	$C[C2 - O2]$	Coordination number between C2 and O2	CV1
	$C[O5 - C2]$	Coordination number between O5 and C2	CV2
	$C[O2 - H_{w,OH}]$	Coordination number between O2 and all the hydrogens of H ₂ O and hydroxyl groups	CV3
F1 → G / G1	$\Delta d[O5 - C1 - O1]$	Distance (in Å) Difference between O5-C1 and C1-O1	CV4
	$C[O5 - C2]$	Coordination number between O5 and C2	CV5
	$C[C2 - O_w]$	Coordination number between C2 and all the oxygens of water	CV6
G1 → G ¹	$\phi[C3 - C2 - C1 - O5]$	Dihedral (in degrees) between atoms C3, C2, C1 and O5	CV52
F1 / F1b → F2	$C[C2 - H2]$	Coordination number between C2 and H	CV16
	$C[O1 - H_{w,OH}]$	Coordination number between O1 and all the hydrogens of H ₂ O and hydroxyl groups	CV17
F2 → F1	$d[C1 - C2]$	Distance (in Å) between C1 and C2	CV18
	$C[C2 - H_{w,OH}]$	Coordination number between C2 and all the hydrogens of H ₂ O and hydroxyl groups	CV19
	$C[O1 - H_{w,OH}]$	Coordination number between O1 and all the hydrogens of H ₂ O and hydroxyl groups	CV20
F2 → F3	$C[C3 - O3]$	Coordination number between C3 and O3	CV21

¹It was found that in SCW, **F1** forms **G1**. Therefore, free energy barrier for **F1**→**G** in SCW was computed by adding the free energy barrier for **G1**→**G** with that of **F1**→**G1**.

	$C[\text{O3} - \text{H}_{\text{w,OH}}]$	Coordination number between O3 and all the hydrogens of H ₂ O and hydroxyl groups	CV22
	$C[\text{O1} - \text{H}_{\text{w,OH}}]$	Coordination number between O1 and all the hydrogens of H ₂ O and hydroxyl groups	CV23
F3→F2	$d[\text{C2} - \text{C3}]$	Distance(in Å) between C2 and C3	CV24
	$C[\text{O1} - \text{H}_{\text{w,OH}}]$	Coordination number between O1 and all the hydrogens of H ₂ O and hydroxyl groups	CV25
	$C[\text{C3} - \text{O}_{\text{w}}]$	Coordination number between C3 and oxygen of all H ₂ O molecules	CV26
F3→H	$C[\text{C5} - \text{H5}]$	Coordination number between C5 and H5	CV27
	$C[\text{C4} - \text{O4}]$	Coordination number between C4 and O4	CV28
	$C[\text{O4} - \text{H}_{\text{w,OH}}]$	Coordination number between O4 and all the hydrogens of H ₂ O and hydroxyl groups	CV29
H→F3	$d[\text{C4} - \text{C5}]$	Distance (in Å) between C4 and C5	CV30
	$C[\text{C5} - \text{H}_{\text{w,OH}}]$	Coordination number between C5 and all the hydrogens of H ₂ O and hydroxyl groups	CV31
	$C[\text{C4} - \text{O}_{\text{w}}]$	Coordination number between C4 and oxygen of all H ₂ O molecules	CV32
G→G3	$\Phi[\text{C3} - \text{C2} - \text{C1} - \text{O5}]$	Dihedral angle (in degrees) between atoms C3, C2, C1 and O5	CV7
	$\Delta C[\text{O2} - \text{C1}, \text{C1} - \text{O1}]$	Difference in coordination number between O2-C1 and C1-O2	CV8

	$C[\text{O1} - \text{H}_{\text{w,OH}}]$	Coordination number between O1 and all the hydrogens of H ₂ O and hydroxyl groups	CV9
G3→G1	$C[\text{C1} - \text{O2}]$	coordination number between C1 and O2	CV10
	$C[\text{C1} - \text{O}_{\text{w}}]$	Coordination number between C1 and all the oxygens of water	CV11
	$C[\text{O1} - \text{H}_{\text{w,OH}}]$	Coordination number between O1 and all the hydrogens of H ₂ O and hydroxyl groups	CV12
G3→F1	$C[\text{O5} - \text{C2}]$	coordination number between O5 and C2	CV13
	$C[\text{C2} - \text{O2}]$	Coordination number between C2 and O2	CV14
	$C[\text{O2} - \text{H}_{\text{w,OH}}]$	Coordination number between O2 and all the hydrogens of H ₂ O and hydroxyl groups	CV15
G→R1	$d[\text{C1} - \text{O5}]$	Distance (in Å) between atoms C1 and O5	CV33
	$C[\text{O1} - \text{H}_{\text{w,OH}}]$	Coordination number between O1 and all the hydrogens of H ₂ O and hydroxyl groups	CV34
	$C[\text{O5} - \text{H}_{\text{w,OH}}]$	Coordination number between O5 and all the hydrogens of H ₂ O and hydroxyl groups	CV35
R1→G1	$C[\text{O1} - \text{H}_{\text{w,OH}}]$	Coordination number between O1 and all the hydrogens of H ₂ O and hydroxyl groups	CV36
	$d[\text{C1} - \text{O5}]$	Distance (in Å) between C1 and O5	CV37
	$C[\text{O5} - \text{H}_{\text{w,OH}}]$	Coordination number between O5 and all the hydrogens of H ₂ O and hydroxyl groups	CV38

R1→R3	$\Delta d[\text{C2} - \text{H2} - \text{C1}]$	Difference between distances (in Å) $d[\text{C2} - \text{H2}]$ and $d[\text{H2} - \text{C1}]$	CV39
	$C[\text{O1} - \text{H}_{\text{w,OH}}]$	Coordination number between O1 and all the hydrogens of H ₂ O and hydroxyl groups	CV40
R3→R1	$C[\text{C1} - \text{H}_{1,2}]$	Coordination number between C1 and H1 and H2	CV41
	$C[\text{C2} - \text{H}_{1,2}]$	Coordination number between C2 and H1 and H2	CV42
	$C[\text{O2} - \text{H}_{\text{w,OH}}]$	Coordination number between O2 and all the hydrogens of H ₂ O and hydroxyl groups	CV43
R3→F	$d[\text{O5} - \text{C2}]$	Distance (in Å) between O5 and C2	CV54
	$C[\text{O2} - \text{H}_{\text{w,OH}}]$	Coordination number between O2 and all the hydrogens of H ₂ O and hydroxyl groups	CV55
	$C[\text{O5} - \text{H}_{\text{w,OH}}]$	Coordination number between O5 and all the hydrogens of H ₂ O and hydroxyl groups	CV56
F→R3	$C[\text{C2} - \text{O5}]$	Coordination number between C2 and O5	CV57
	$C[\text{O2} - \text{H}_{\text{w,OH}}]$	Coordination number between O2 and all the hydrogens of H ₂ O and hydroxyl groups	CV58
	$C[\text{O5} - \text{H}_{\text{w,OH}}]$	Coordination number between O5 and all the hydrogens of H ₂ O and hydroxyl groups	CV59
F→F1b	$C[\text{C2} - \text{H}_{1,2}]$	Coordination number between C2 and H1,H2	CV66
	$C[\text{C2} - \text{O2}]$	Coordination number between C2 and O2	CV67

	$C[\text{O2} - \text{H}_{\text{w,OH}}]$	Coordination number between O2 and all the hydrogens of H ₂ O and hydroxyl groups	CV68
F1b→F	$\Delta d[\text{C2} - \text{H2} - \text{C1}]$	Difference between distances (in Å) $d[\text{C2} - \text{H2}]$ and $d[\text{H2} - \text{C1}]$	CV69
	$C[\text{O1} - \text{H}_{\text{w,OH}}]$	Coordination number between O1 and all the hydrogens of H ₂ O and hydroxyl groups	CV70
	$C[\text{C2} - \text{O}_{\text{w}}]$	Coordination number between C2 and oxygen of all the water molecules	CV71
R1→R2	$C[\text{C2} - \text{H2}]$	Coordination number between C2 and H2	CV44
	$C[\text{O1} - \text{H}_{\text{w,OH}}]$	Coordination number between O1 and all the hydrogens of H ₂ O and hydroxyl groups	CV45
R2→R1	$d[\text{C1} - \text{C2}]$	Distance (in Å) between C1 and C2	CV46
	$C[\text{C2} - \text{H}_{\text{w,OH}}]$	Coordination between C2 and all the hydrogens of H ₂ O and hydroxyl groups	CV47
	$C[\text{O1} - \text{H}_{\text{w,OH}}]$	Coordination number between O1 and all the hydrogens of H ₂ O and hydroxyl groups	CV48
R2→R3	$d[\text{C1} - \text{C2}]$	Distance (in Å) between C1 and C2	CV49
	$C[\text{C1} - \text{H}_{\text{w,OH}}]$	Coordination number between C1 and all the hydrogens of H ₂ O and hydroxyl groups	CV50
	$C[\text{O2} - \text{H}_{\text{w,OH}}]$	Coordination number between O2 and all the hydrogens of H ₂ O and hydroxyl groups	CV51

R1→R5	$C[C2 - H]$	Coordination number between C2 and H of C2	CV60
	$C[C3 - O3]$	Coordination number between C3 and O3	CV61
	$C[O3 - H_{w,OH}]$	Coordination number between O3 and all the hydrogens of H ₂ O and hydroxyl groups	CV62

4 Free energy barriers and reconstructed free energy surfaces

4.1 Free energy barriers

Table S4: Free energy barriers, ΔF^\ddagger (in kcal mol⁻¹) of elementary steps

Reaction	ΔF^\ddagger	
	ABW	SCW
G→F1	48	37
F1→G	43	43
F1→F2	30	32
F2→F1	27	24
F2→F3	14	21
F3→F2	31	33
F3→H	18	21
H→F3	62	72
G→G3	33	29
G3→G	26	31
G3→F1	35	32
G→R1	24	24
R1→G1	18	21
G1→G	7	4
R1→R3	20	21
R3→R1	33	32
R3→F	19	20
F→R3	22	28
F→F1b	34	35

F1b→F	28	27
F1b→F2	35	37
R1→R2	27	33
R2→R1	25	30
R2→R3	23	27
R1→R5	35	39

4.2 Reconstructed free energy surfaces for reactions in ABW

4.2.1 Cy1 Pathway

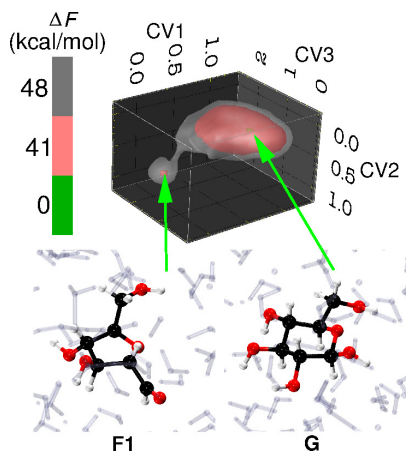


Figure S2: Reconstructed free energy surface for the reaction $G \rightarrow F1$.

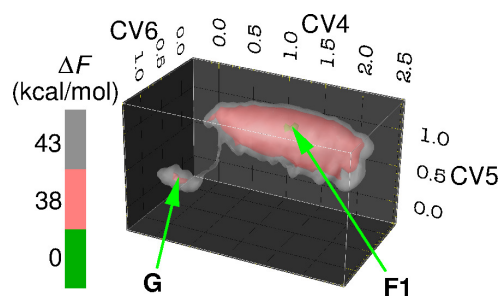


Figure S3: Reconstructed free energy surface for the reaction $F1 \rightarrow G$.

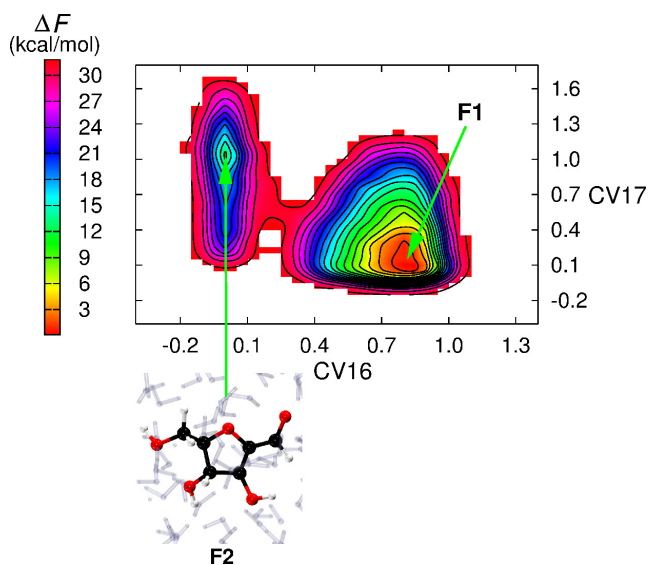


Figure S4: Reconstructed free energy surface for the reaction $F1 \rightarrow F2$.

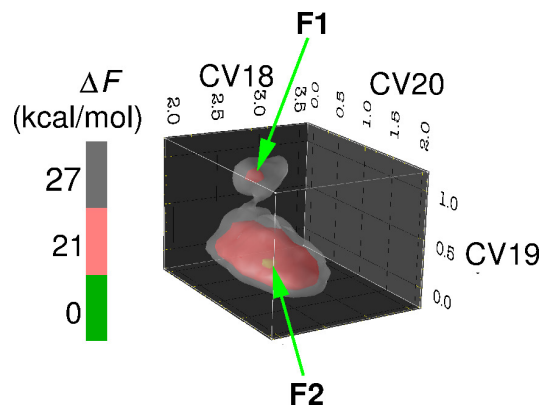


Figure S5: Reconstructed free energy surface for the reaction $F2 \rightarrow F1$.

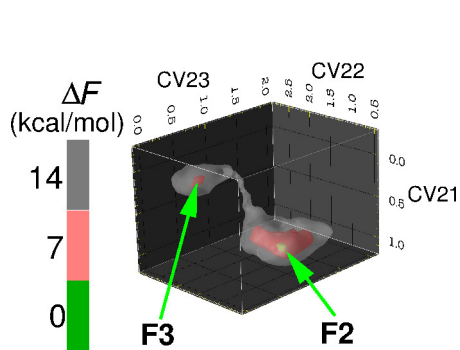


Figure S6: Reconstructed free energy surface for the reaction **F2**→**F3**.

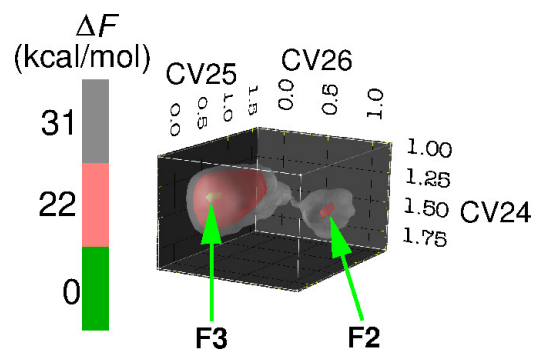


Figure S7: Reconstructed free energy surface for the reaction **F3**→**F2**.

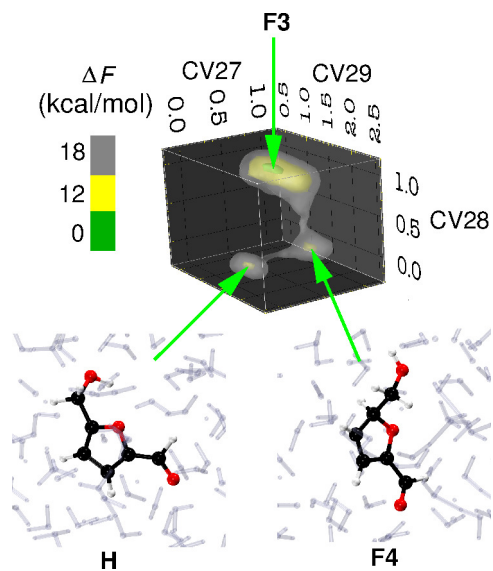


Figure S8: Reconstructed free energy surface for the reaction **F3**→**H**.

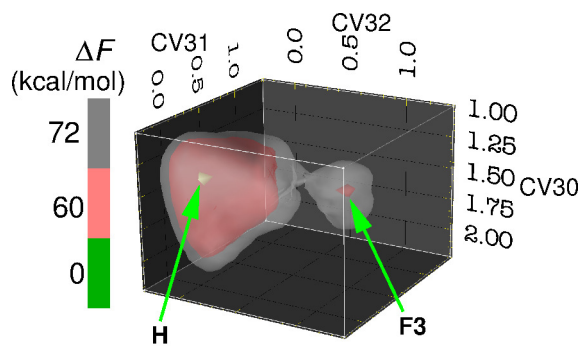


Figure S9: Reconstructed free energy surface for the reaction **H**→**F3**.

4.2.2 Cy2 pathway

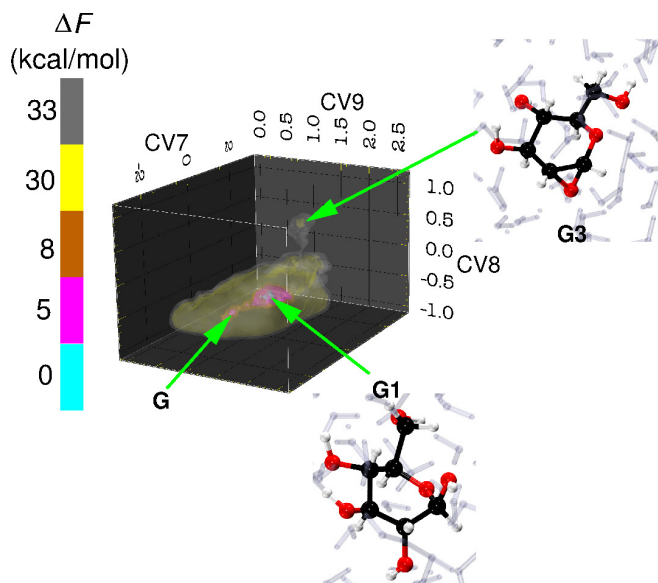


Figure S10: Reconstructed free energy surface for the reaction $G \rightarrow G3$.

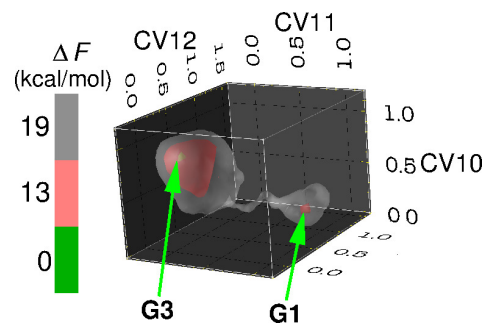


Figure S11: Reconstructed free energy surface for the reaction $G3 \rightarrow G1$.

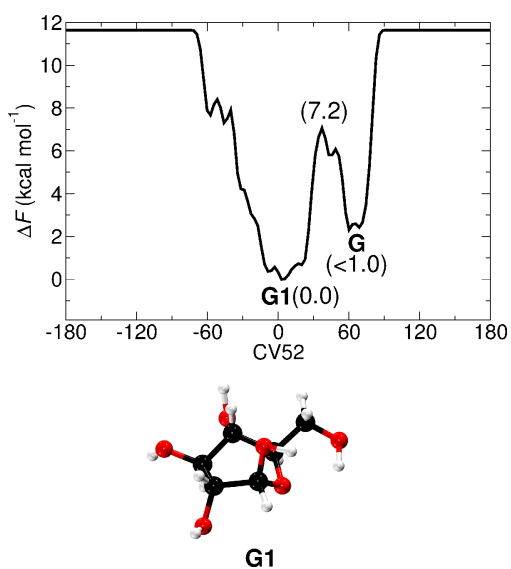


Figure S12: Free energy curve for $G1 \rightarrow G$ conversion.

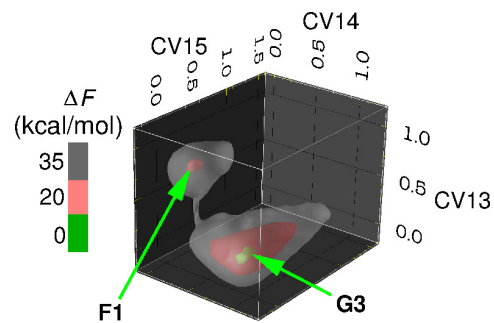


Figure S13: Reconstructed free energy surface for the reaction $G3 \rightarrow F1$.

4.2.3 ACy1 pathway

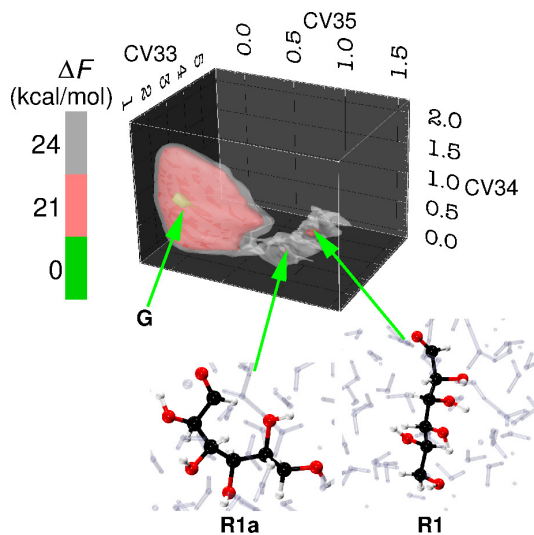


Figure S14: Reconstructed free energy surface for the reaction $G \rightarrow R1$.

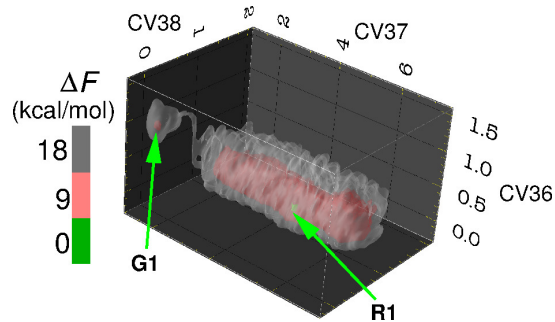


Figure S15: Reconstructed free energy surface for the reaction $R1 \rightarrow G1$.

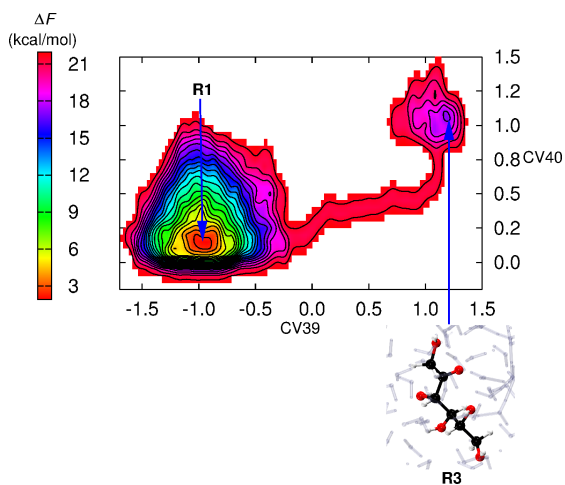


Figure S16: Reconstructed free energy surface for the reaction $R1 \rightarrow R3$.

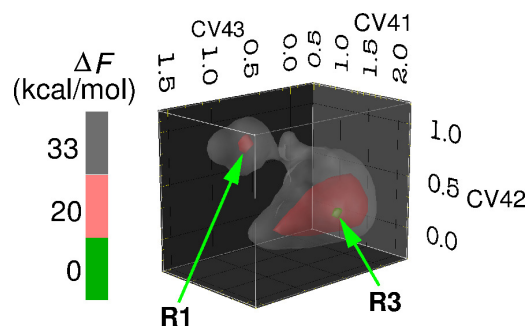


Figure S17: Reconstructed free energy surface for the reaction $R3 \rightarrow R1$.

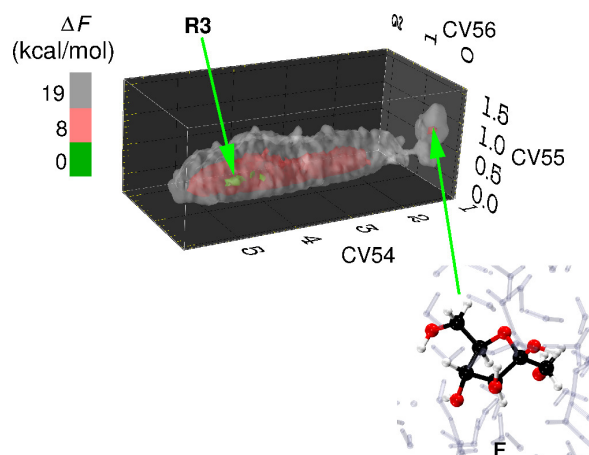


Figure S18: Reconstructed free energy surface for the reaction **R3**→**F**.

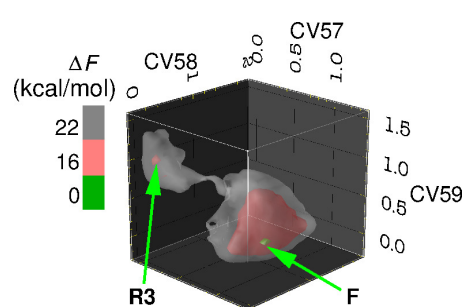


Figure S19: Reconstructed free energy surface for the reaction **F**→**R3**.

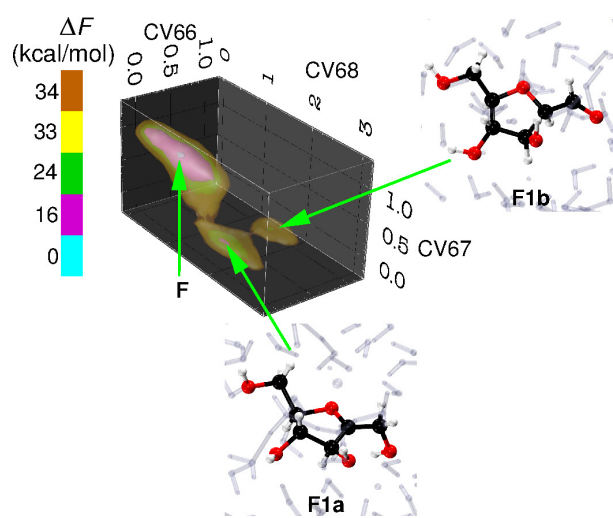


Figure S20: Reconstructed free energy surface for the reaction **F**→**F1b**.

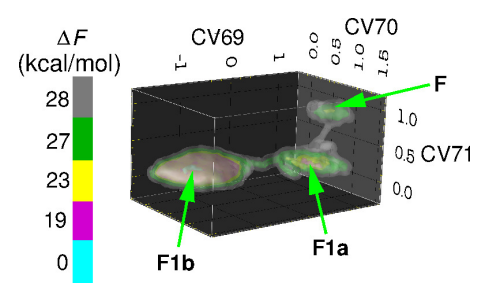


Figure S21: Reconstructed free energy surface for the reaction **F1b**→**F**.

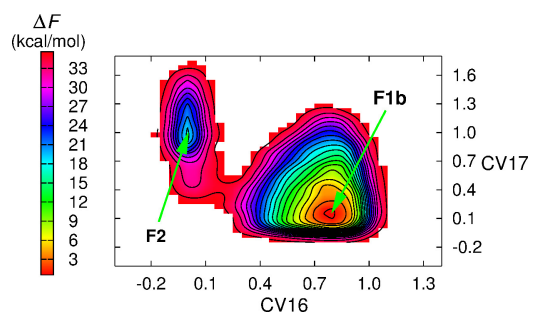


Figure S22: Reconstructed free energy surface for the reaction $\mathbf{F1b} \rightarrow \mathbf{F2}$.

4.2.4 ACy2 Pathway

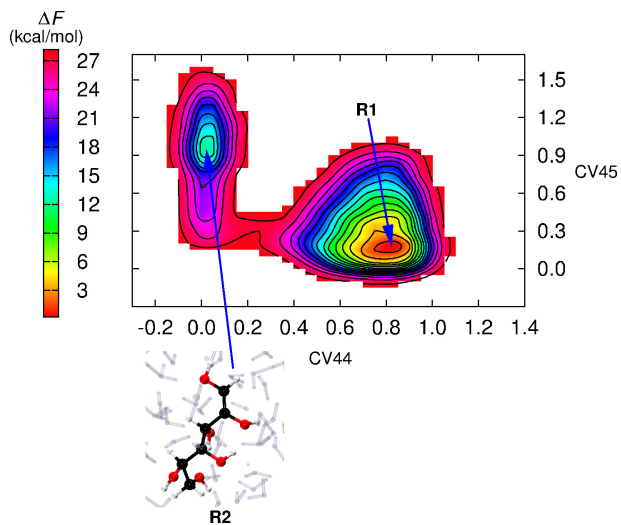


Figure S23: Reconstructed free energy surface for the reaction **R1**→**R2**.

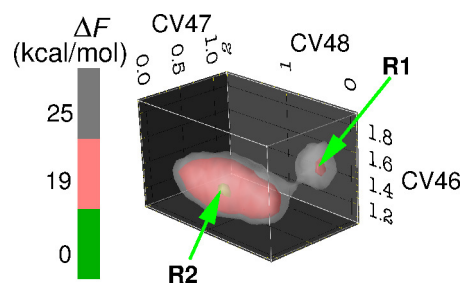


Figure S24: Reconstructed free energy surface for the reaction **R2**→**R1**.

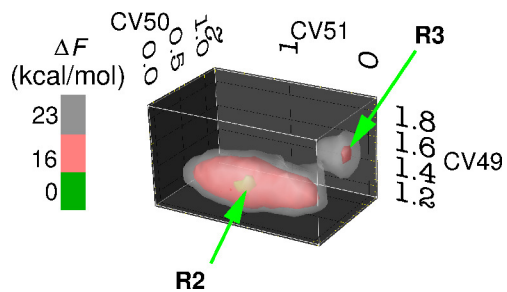


Figure S25: Reconstructed free energy surface for the reaction **R2**→**R3**.

4.2.5 ACy3 pathway

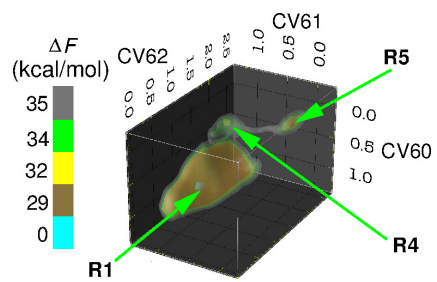


Figure S26: Reconstructed free energy surface for the reaction **R1**→**R5**.

4.3 Reconstructed free energy surfaces for reactions in SCW

4.3.1 Cy1 pathway

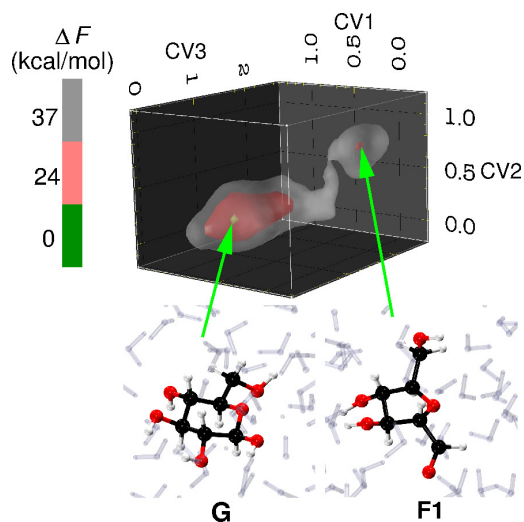


Figure S27: Reconstructed free energy surface for the reaction $G \rightarrow F1$.

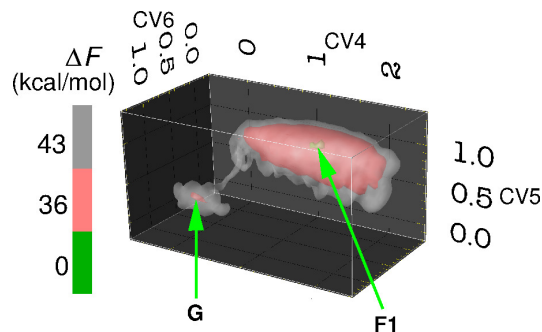


Figure S28: Reconstructed free energy surface for the reaction $F1 \rightarrow G$.

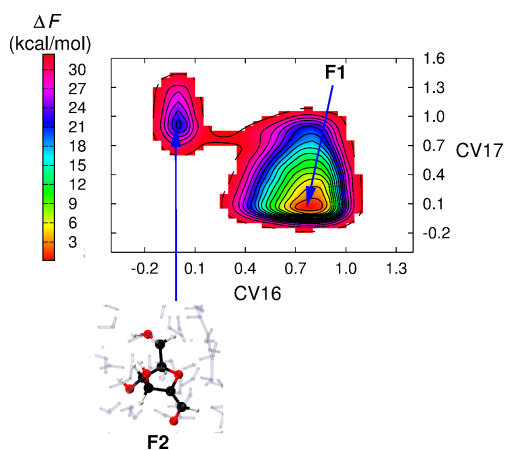


Figure S29: Reconstructed free energy surface for the reaction $F1 \rightarrow F2$.

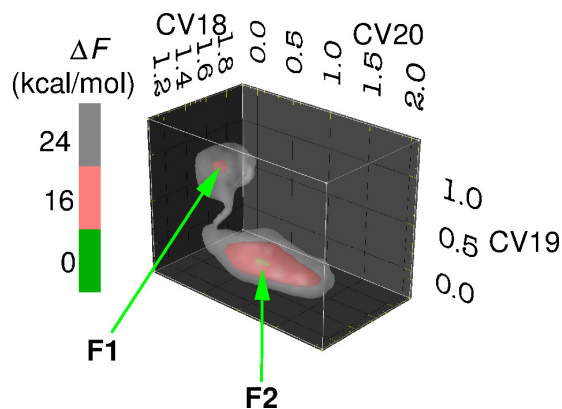


Figure S30: Reconstructed free energy surface for the reaction $F2 \rightarrow F1$.

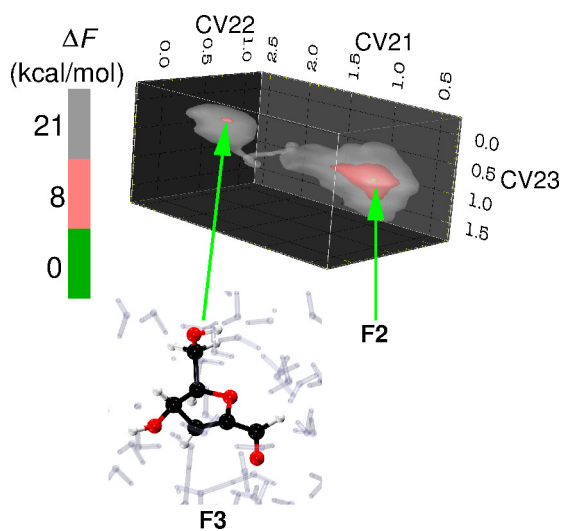


Figure S31: Reconstructed free energy surface for the reaction **F2**→**F3**.

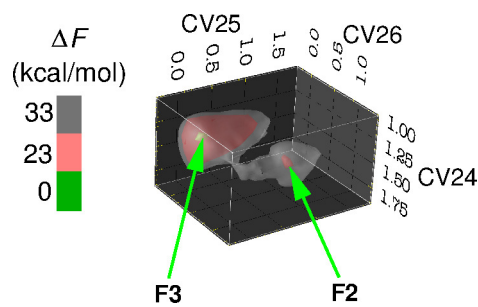


Figure S32: Reconstructed free energy surface for the reaction **F3**→**F2**.

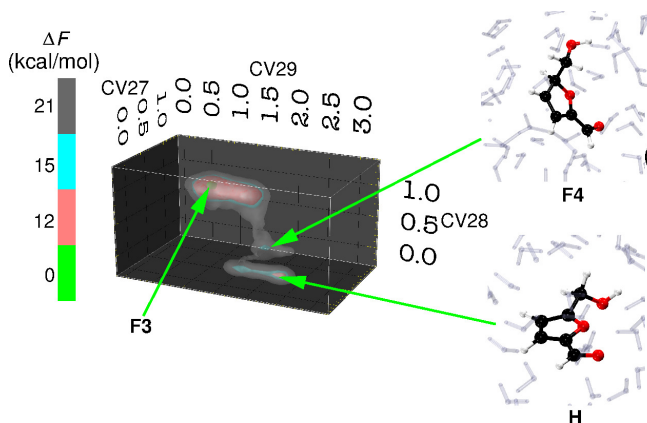


Figure S33: Reconstructed free energy surface for the reaction **F3**→**H**.

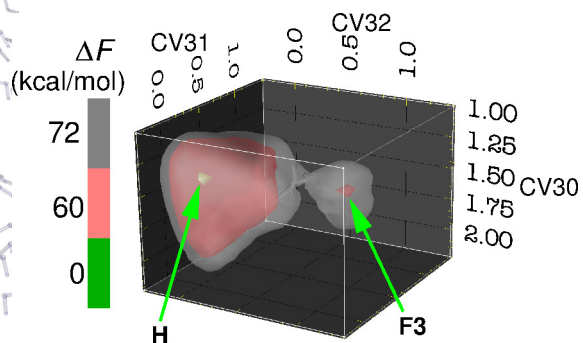


Figure S34: Reconstructed free energy surface for the reaction **H**→**F3**.

4.3.2 Cy2 pathway

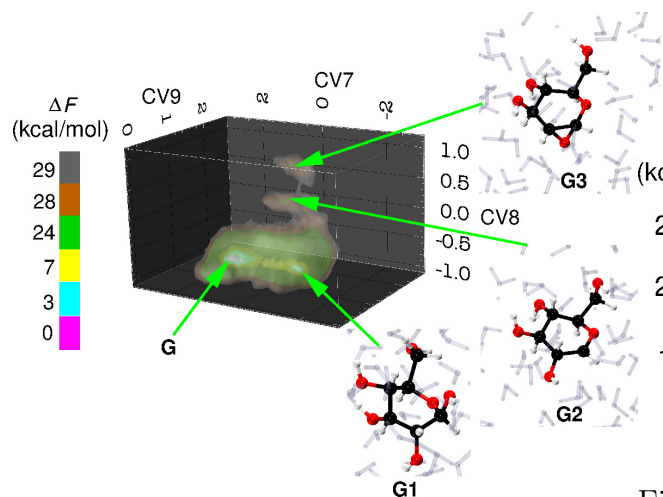


Figure S35: Reconstructed free energy surface for the reaction $\mathbf{G} \rightarrow \mathbf{G3}$.

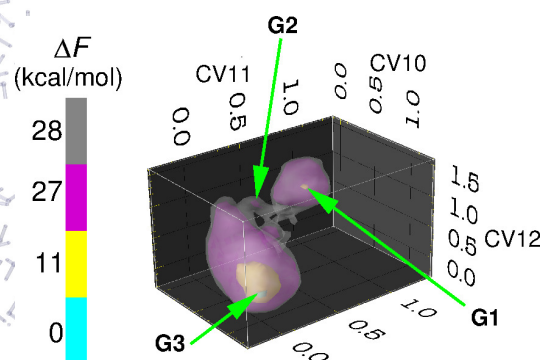


Figure S36: Reconstructed free energy surface for the reaction $\mathbf{G3} \rightarrow \mathbf{G1}$.

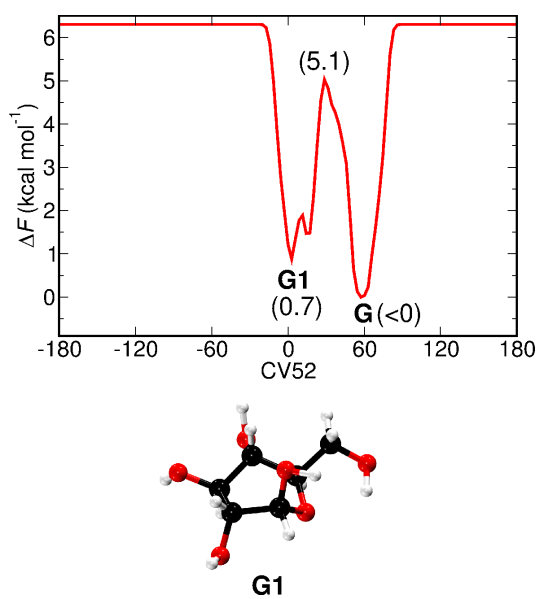


Figure S37: Free energy curve for $\mathbf{G1} \rightarrow \mathbf{G}$ conversion.

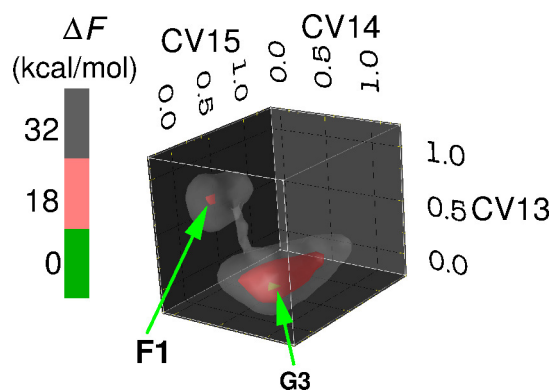


Figure S38: Reconstructed free energy surface for the reaction $\mathbf{G3} \rightarrow \mathbf{F1}$.

4.3.3 ACy1 pathway

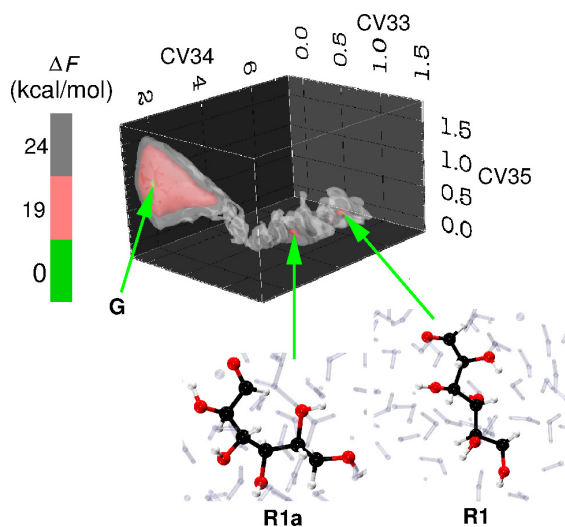


Figure S39: Reconstructed free energy surface for the reaction $G \rightarrow R1$.

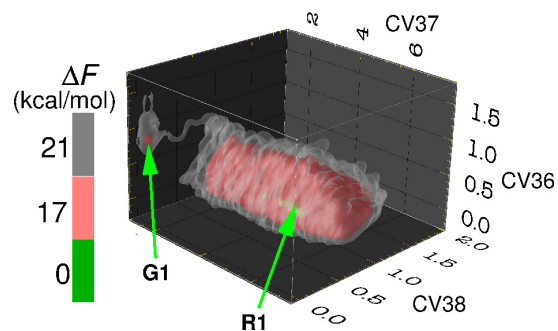


Figure S40: Reconstructed free energy surface for the reaction $R1 \rightarrow G1$.

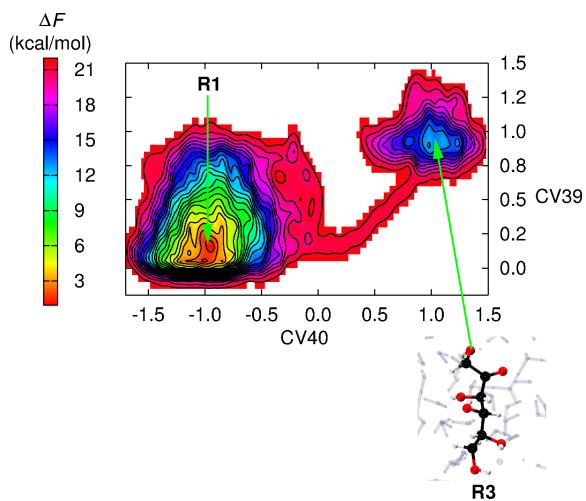


Figure S41: Reconstructed free energy surface for the reaction $R1 \rightarrow R3$.

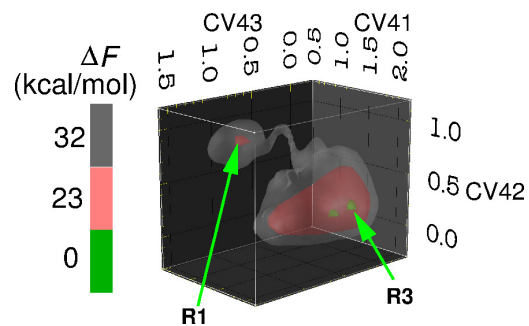


Figure S42: Reconstructed free energy surface for the reaction $R3 \rightarrow R1$.

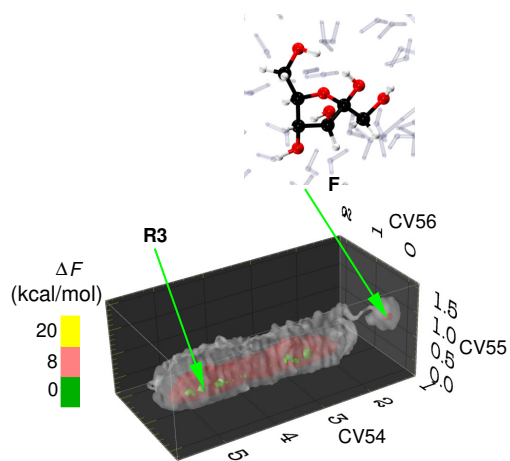


Figure S43: Reconstructed free energy surface for the reaction **R3**→**F**.

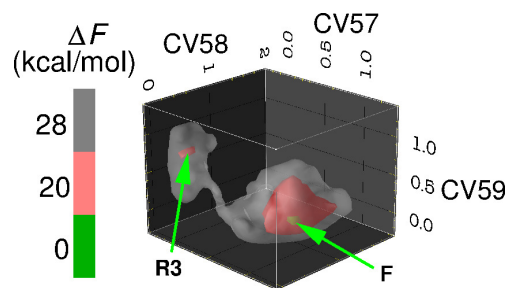


Figure S44: Reconstructed free energy surface for the reaction **F**→**R3**.

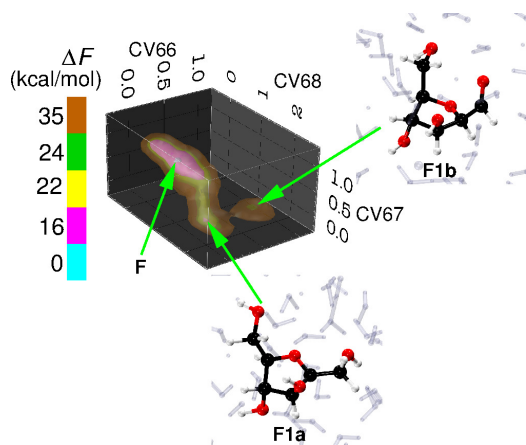


Figure S45: Reconstructed free energy surface for the reaction **F**→**F1b**.

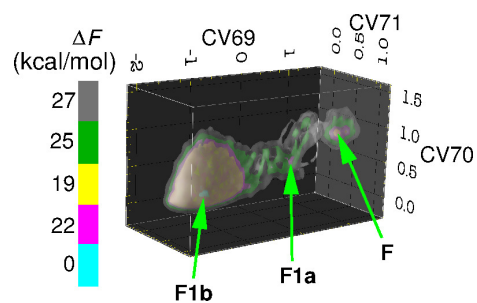


Figure S46: Reconstructed free energy surface for the reaction **F1b**→**F**.

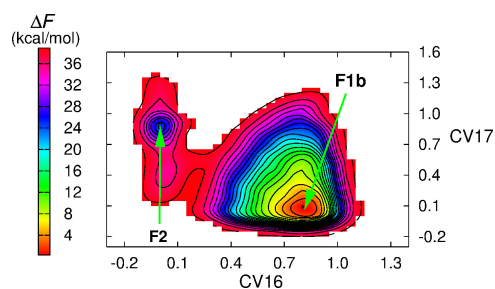


Figure S47: Reconstructed free energy surface for the reaction **F1b**→**F2**.

4.3.4 ACy2 pathway

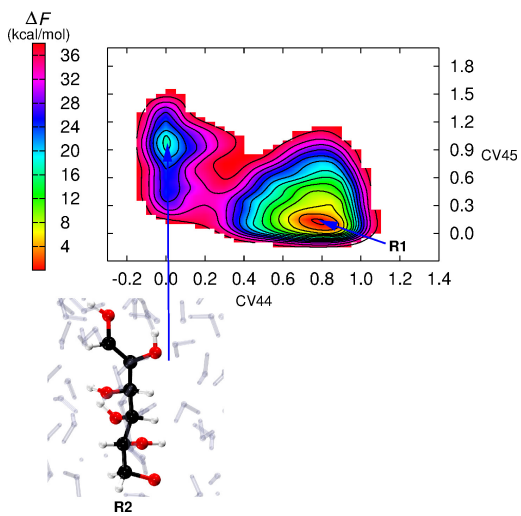


Figure S48: Reconstructed free energy surface for the reaction **R1**→**R2**.

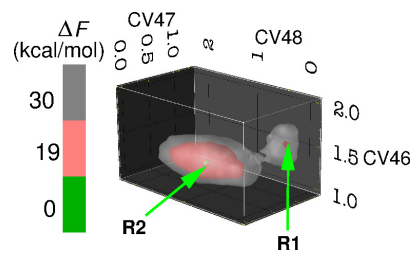


Figure S49: Reconstructed free energy surface for the reaction **R2**→**R1**.

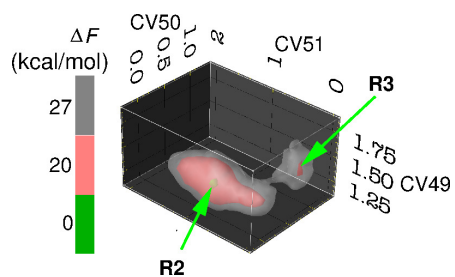


Figure S50: Reconstructed free energy surface for the reaction **R2**→**R3**.

4.3.5 ACy3 pathway

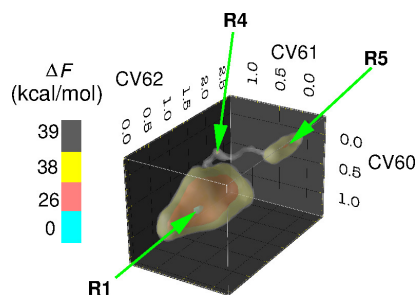


Figure S51: Reconstructed free energy surface for the reaction **R1**→**R5**.

5 Effect of intra-molecular hydrogen bond interactions

Analysis of elementary reactions along all the pathways indicates that intra-molecular hydrogen bond interactions can act as both facilitators and retardant depending on the nature of the reaction. For example, during **F**→**R3** and **F2**→**F3** these interactions result in an increase in free energy barrier whereas for **F2**→**F1** they have the opposite effect. Formation of **R3** from **F** (see Figure 5) involves the cleavage of O5–C2 bond after the protonation of O5 by bulk water molecules. It was found that the free energy barrier for this reaction in SCW is about 6 kcal mol^{-1} higher than that in ABW. Metadynamics simulations indicate the presence of stable intra-molecular interactions between O5 of **F1** and the hydrogens (H6a and H1a) of neighboring $-\text{CH}_2\text{OH}$ groups in SCW, whereas number of such interactions are found to be lesser in ABW than that in SCW (Figure S52 (c), (d)), especially the strong hydrogen bond interactions (Figure S52 (a), (b)). Since protonation at O5 by bulk water assists the O5–C2 bond cleavage, the intra-molecular interactions between O5 and hydrogens (H6a and H1a) which reduce accessibility of bulk water by interacting with the lone pairs of O5 is expected to slow down the reaction in SCW. It was also noted that near to the TS, number of such intra-molecular interactions were found to be decreasing. Therefore, the higher free energy barrier for **F**→**R3** in SCW compared to ABW can be ascribed to the

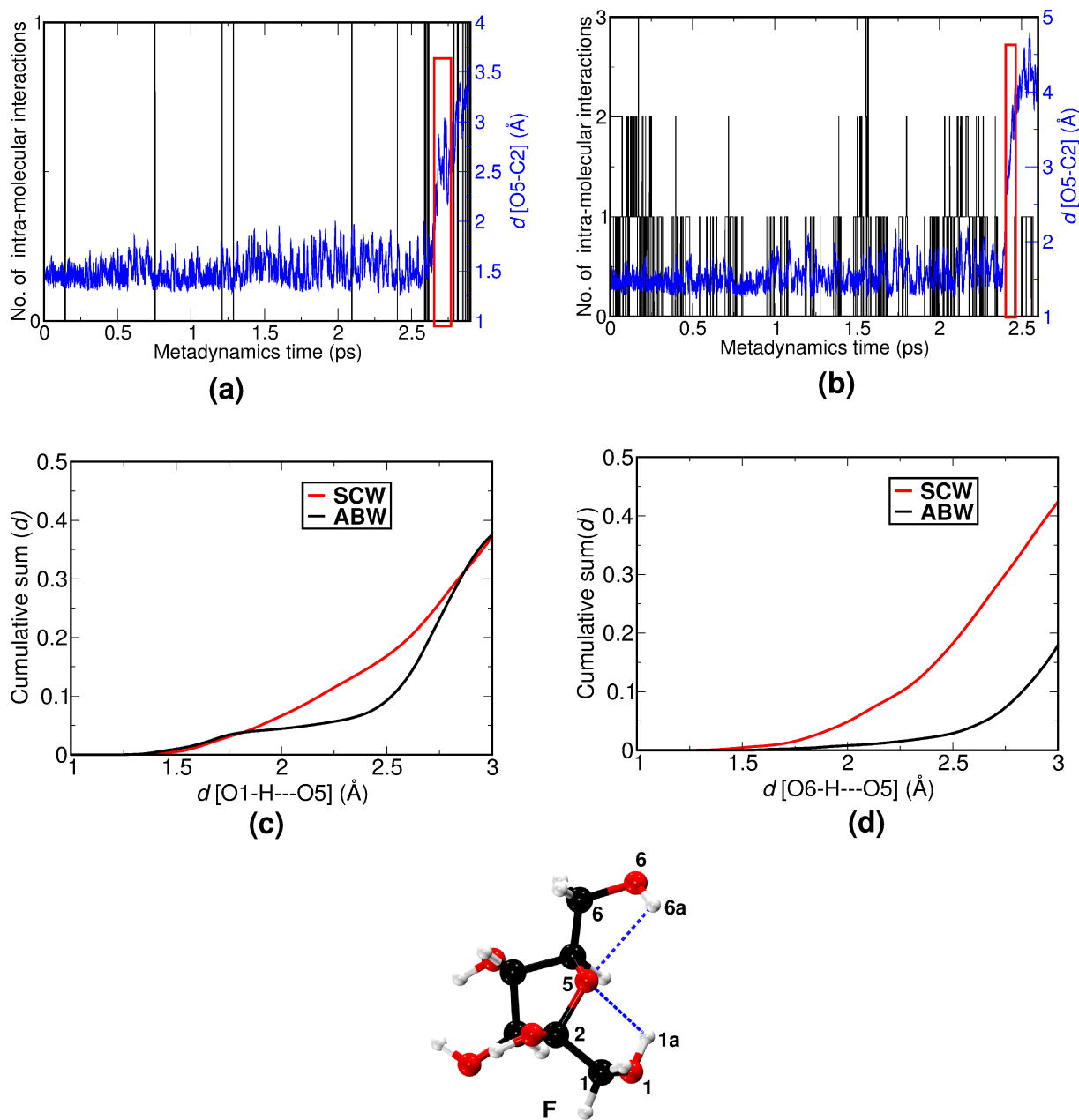


Figure S52: (a),(b) Number of intra-molecular hydrogen bond interactions (black curve and left Y-axis) and distance (in Å) between atoms O5 and C2, $d[\text{O5} - \text{C2}]$ (blue curve and right Y-axis) as a function of metadynamics time in ABW and SCW, respectively. The approximate transition region is highlighted by red rectangles. Cumulative sum of number of intra-molecular hydrogen bonding interaction as a function of distance (in Å) between O5 and (c) H1a (hydrogen of O1), $d[\text{O1} - \text{H} \cdots \text{O5}]$ and (d) H6a, $d[\text{O6} - \text{H} \cdots \text{O5}]$ in ABW (black curve) and in SCW (red curve) for step **F** \rightarrow **R3**. Here, intra-molecular interactions are counted after neglecting the angle cut-off used to determine hydrogen bonding shown in Figure 10 of the manuscript.

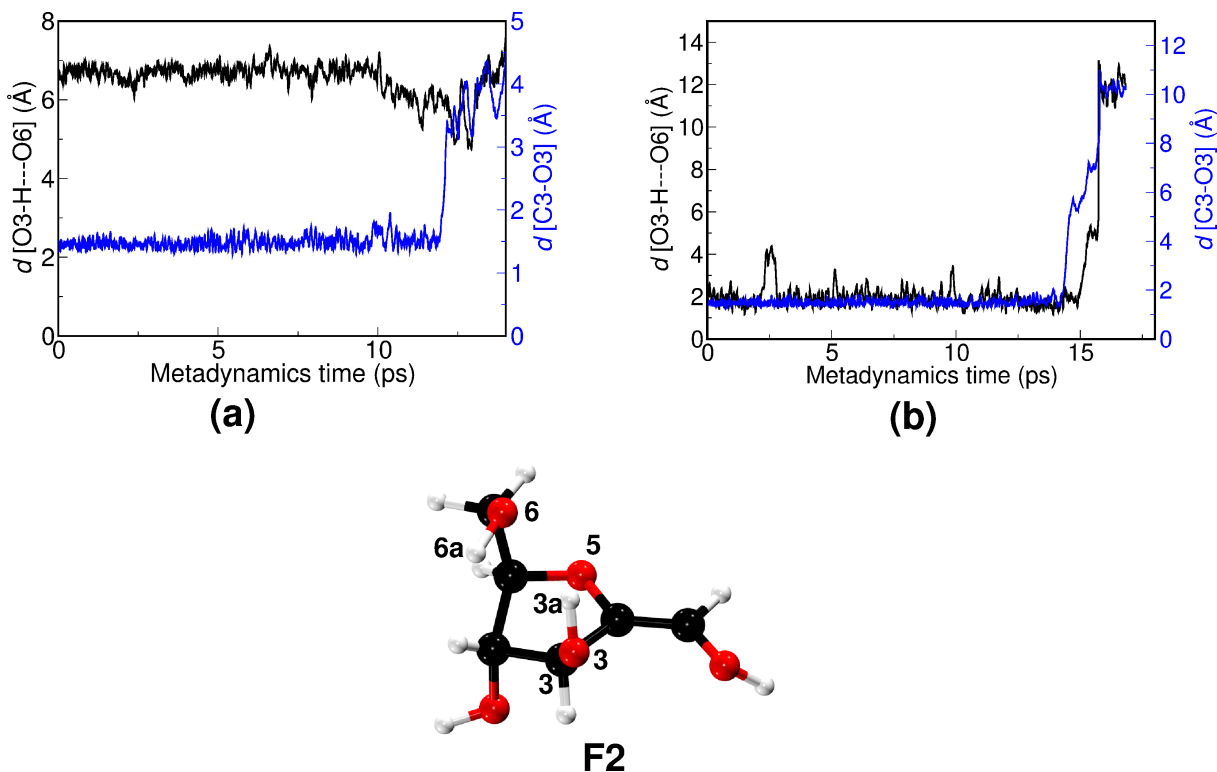


Figure S53: Distance (Å) between H3a (hydrogen of O3) and O6, $d[\text{O3} - \text{H}\cdots\text{O6}]$ (black curve and left Y-axis) and distance (Å) between C3 and O3, $d[\text{C3} - \text{O3}]$ (blue curve and right Y-axis) as a function of metadynamics time for step **F2**→**F3** in (a) ABW and (b) SCW.

stabilization of **F** and to the diminished affinity of O5 to get protonated.

Step **F2**→**F3** is the acid catalyzed dehydration at C3. It was found that in SCW the free energy barrier for this reaction is about 7 kcal mol^{-1} higher than that in ABW (21 and 14 kcal mol^{-1} , respectively). Our analysis indicated the presence of intra-molecular interactions between O6 and H3a (hydrogen of the hydroxyl group at C3) in SCW which is absent in ABW (Figure S53). The intra-molecular interactions between O3 and H6a in SCW hinder the protonation of O3 by bulk water molecules, which in turn prevent the dehydration at C3. These interactions are expected to slow down the reaction in SCW. Also, these interactions can stabilize the reactant state. Since these interactions are absent in the TS, in addition to the fact that the dehydration is slowed down due to intra-molecular interactions, the stabilization of reactant is also responsible for the higher free energy barrier

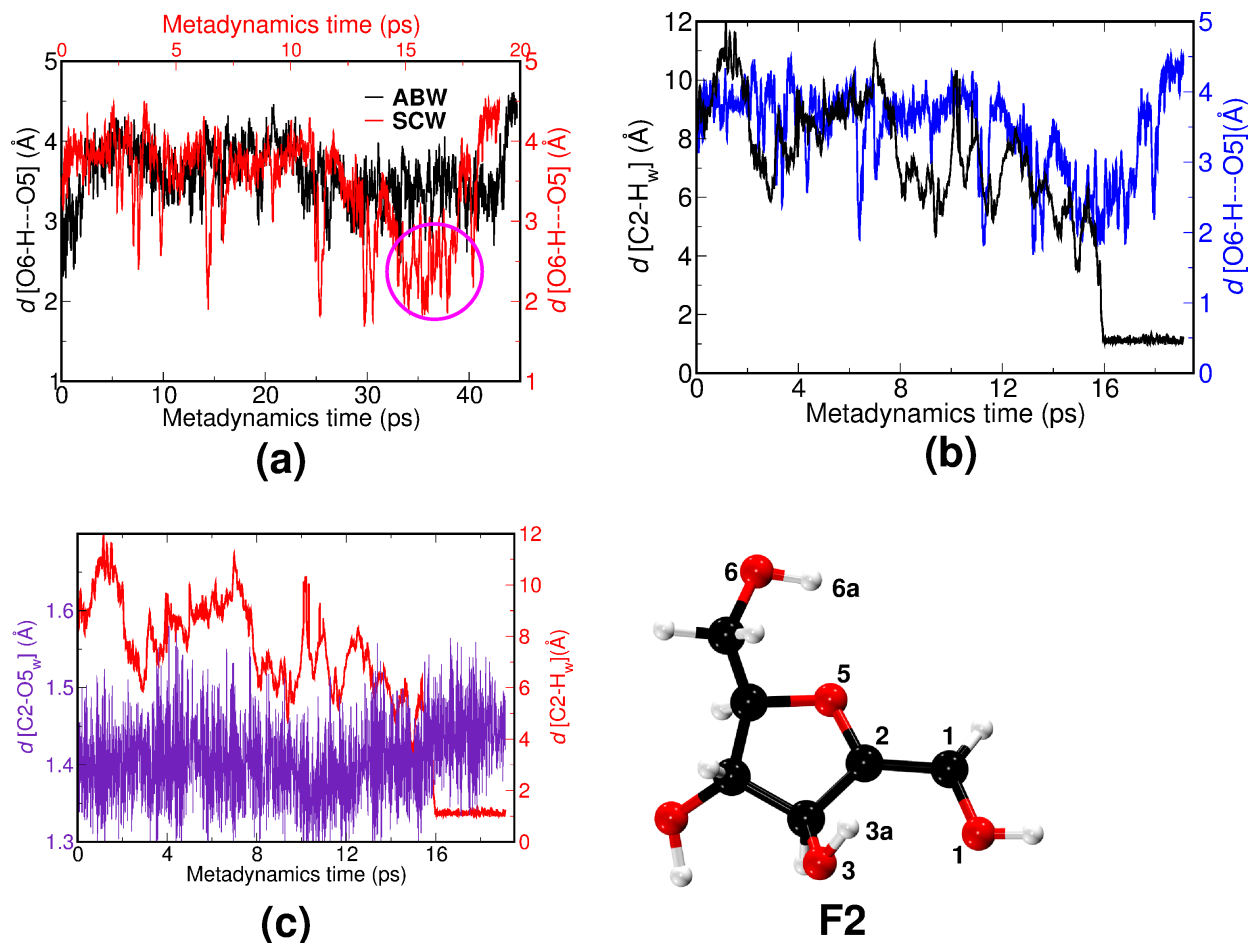


Figure S54: (a) Distance between H6a and O5 ($d[\text{O6} - \text{H} \cdots \text{O5}]$) as a function of metadynamics time under ABW (black curve and left Y-axis) and SCW (red curve and axis labels) for step **F2**→**F1**. The magenta circle indicates the region where intra-molecular interaction becomes prominent in SCW (b) $d[\text{O6} - \text{H} \cdots \text{O5}]$ (blue curve and right Y-axis) and distance between C2 and bulk water hydrogen (H_w), $d[\text{C2} - \text{H}_w]$ (black curve and left Y-axis) for reaction in SCW (c) $d[\text{C2} - \text{H}_w]$ (red curve and right Y-axis) and change in O5–C2 distance, $d[\text{C2} - \text{O5}]$, (violet curve and left Y-axis) as a function of metadynamics time for reaction in SCW. All the distances are in Å.

in SCW compared to that in ABW. Similar observations are also found in other elementary steps such as **G3**→**G** and **F1/F1b**→**F2** and **H**→**F3**, where the free energy barrier in SCW is higher than that in ABW.

In contrast to the previous examples, intra-molecular interactions were found to assist **F2**→**F1** in SCW. Here, the tautomer **F2** undergoes protonation at C2 to form **F1** (see Figure 3). In this case, the lower free energy barrier for reactions in SCW can be ascribed to

the activation of the double bond between C1 and C2 by weakening O5–C2 bond due to the intra-molecular interactions between H6a and O5 (Figure S54), which are absent in ABW. It was also noted that for many reactions where the groups such as –CHO or –OH, protonation of which facilitates the reaction, are not involved in any intra-molecular interactions in SCW, free energy barriers are comparable in ABW and SCW. The comparable free energy barriers (20 and 21 kcal mol⁻¹ in ABW and SCW, respectively) for **R1**→**R3**, where the reaction is facilitated by the protonation of O1 of **R1** which is not involved in any intramolecular interactions in SCW, is an example of this (Figure S55).

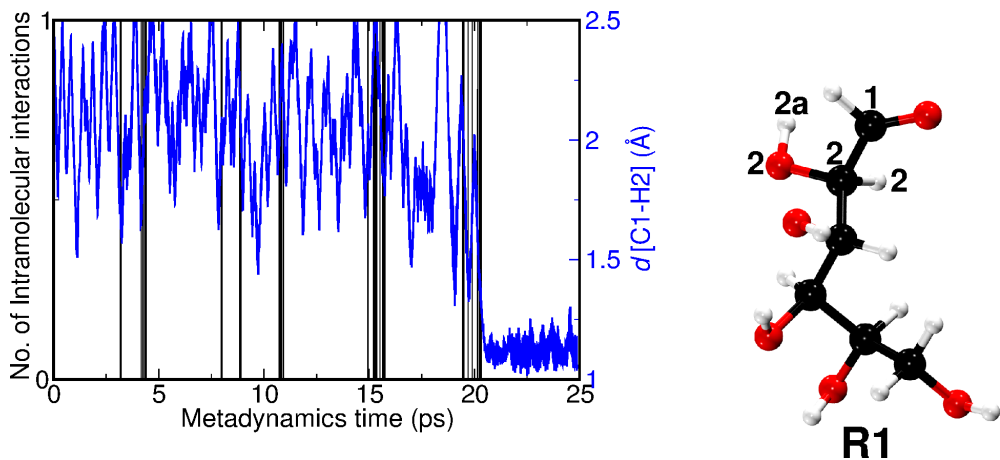


Figure S55: (a) Intra-molecular hydrogen bonding like interaction involving O1 (black curve and left Y-axis) and distance (in Å) between H2 and C1, $d[\text{C1}-\text{H2}]$ (blue curve and right Y-axis) as a function of metadynamics time for step **R1**→**R3** in SCW.

6 Accuracy of PBE functional

In order to estimate the error due to PBE functional,¹ we have computed the free energy barrier for one of the rate determining steps along the **ACy1** pathway, **G**→**R1**, using M06-2X/6-31+G(d,p) level of theory² and compared it with that of PBE/6-31+G(d,p) level of theory. A system consisting of **G** and H₃O⁺ ion is taken as the reactant molecule. Here, the transition state (TS) is modeled by considering that the protonation at O5 occurs prior to the ring opening as observed in our metadynamics simulations. PCM (Polarizable Continuum

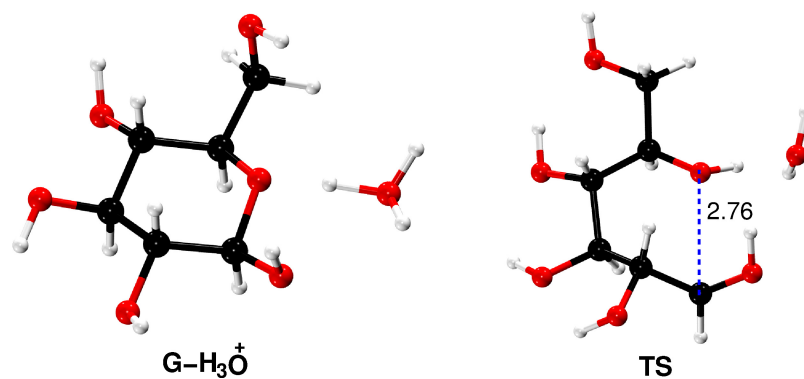


Figure S56: Optimized structures of $\mathbf{G-H_3O^+}$ and \mathbf{TS} obtained using M06-2X/6-31+G(d,p) level of theory with important distance (in Å) labeled.

Model) solvent model³ with water as solvent was used to provide the solvent environment. Bondi's atomic radii⁴ which treat all the atoms of the molecules explicitly was used along with PCM. The level of theory and solvent model used here was used in earlier studies which

Table S5: Free energies, G (a.u.) of $\mathbf{G-H_3O^+}$ and transition state of step $\mathbf{G1} \rightarrow \mathbf{R1}$ (\mathbf{TS}) in ABW and SCW obtained using PBE/6-31+G(d,p) and M06-2X/6-31+G(d,p) level of theories.

	ABW		SCW	
	PBE	M06-2X	PBE	M06-2X
$\mathbf{G-H_3O^+}$	-763.114834	-763.645241	-763.142561	-763.671179
\mathbf{TS}	-763.081462	-763.607718	-763.109993	-763.635853

looked at the various possible dehydration routes of protonated β -D-glucose and was found to have accuracy comparable to that of MP2.⁵

All the computations were performed using Gaussian 09 suite of programs.⁶ Geometry optimization of reactant and transition states in implicit solvent were carried out using the GEDIIS⁷ approach as implemented in Gaussian 09 package. To ascertain the nature of minima and TS, normal mode analysis was performed. The nature of TS was further confirmed by the presence of a single imaginary mode. Here, free energies were computed at both the thermodynamic conditions (ABW and SCW) and the computed free energy values include zero-point correction as well as thermal correction to enthalpy and entropy.

It can be seen from Table S6 that PBE functional underestimates the free energy by about 2.6 kcal mol⁻¹ in ABW condition and 2.2 kcal mol⁻¹ in SCW.

Table S6: Free energy barriers, ΔG^\ddagger (in kcal mol⁻¹) for **G1**→**R1** in ABW and SCW obtained using PBE/6-31+G(d,p) and M06-2X/6-31+G(d,p) level of theories.

	PBE	M06-2X
ABW	20.9	23.5
SCW	20.4	22.2

7 Accuracy of metadynamics simulations

The accuracy of the metadynamics simulation was verified by recomputing the free energy barriers for the steps **G**→**F1** and **G**→**R1** with Gaussian potential heights of 0.38 and 0.19 kcal mol⁻¹ and comparing these barriers with that obtained for a Gaussian potential height of 0.63 kcal mol⁻¹. We have performed these simulations for both ABW and SCW conditions. The reconstructed free energy surfaces from these calculations are given in Figure S57 and Figure S58. The results show that the free energy barriers are converged to 1-2 kcal mol⁻¹ for ABW and SCW conditions with 0.63 kcal mol⁻¹; See Table S7.

Table S7: Free energy barriers (ΔF^\ddagger) for the steps **G**→**F1** and **G**→**R1** at ABW and SCW conditions for different Gaussian potential heights (w).

w (kcal mol ⁻¹)	ΔF^\ddagger (kcal mol ⁻¹)			
	G → F1		G → R1	
	ABW	SCW	ABW	SCW
0.63	48	37	24	24
0.38	46	37	26	23
0.19	47	37	26	23

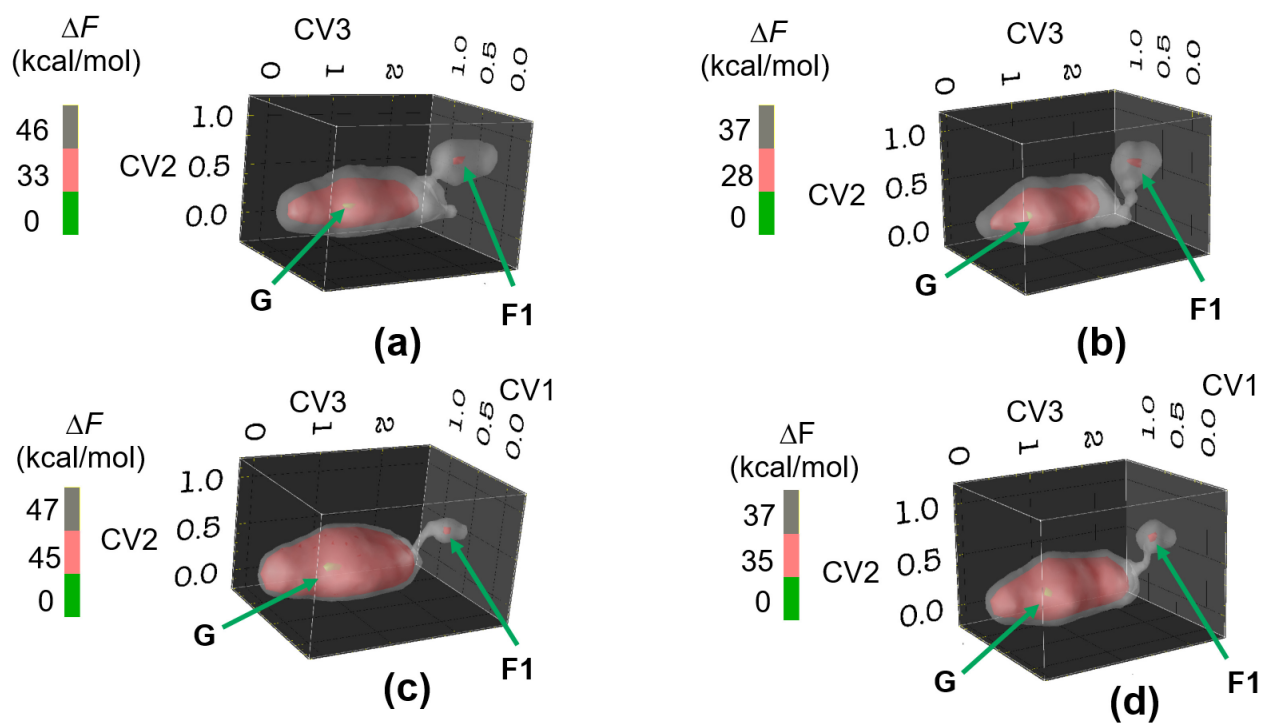


Figure S57: Reconstructed free energy surface for the reaction $G \rightarrow F1$ at (a) ABW (b) SCW conditions computed with Gaussian potential height of $0.38 \text{ kcal mol}^{-1}$ and (c) ABW (d) SCW conditions computed with Gaussian potential height of $0.19 \text{ kcal mol}^{-1}$.

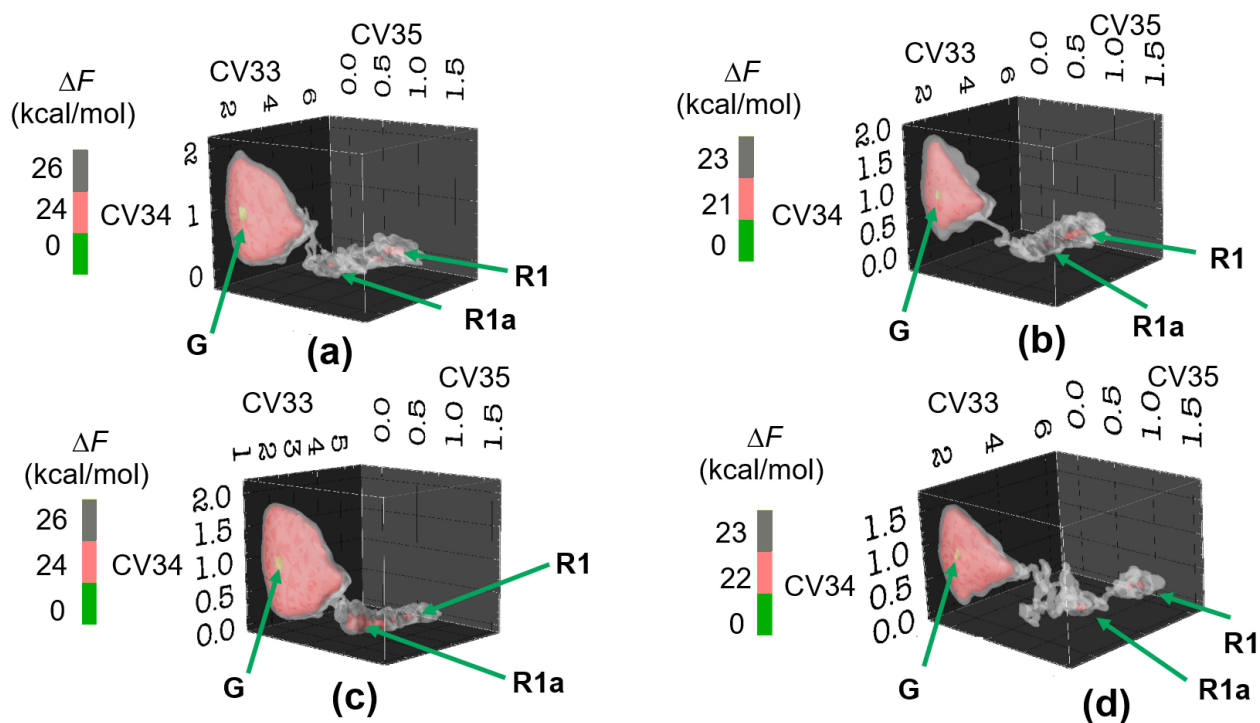


Figure S58: Reconstructed free energy surfaces for $\mathbf{G} \rightarrow \mathbf{R1}$ at (a) ABW (b) SCW conditions computed using Gaussian potential height of $0.38 \text{ kcal mol}^{-1}$ and (c) ABW (d) SCW conditions computed with Gaussian potential height of $0.19 \text{ kcal mol}^{-1}$.

8 Analysis of ring flipping conformations during step $\mathbf{G} \rightarrow \mathbf{G3}$

The collective coordinate $\Phi[\text{C3-C2-C1-O5}]$ was found to aid in sampling various conformational states of \mathbf{G} due to ring puckering. Figure S59 shows the snapshots of the conformational states observed during the simulation. To further quantify, we chose all the energy-minimized conformations of ring puckered states as reported in the work of Biarnés et al.⁸ as the reference and computed the root mean square deviation (RMSD) of the metadynamics trajectory (excluding the exo-cyclic groups); see Figure S60. We noticed that RMSD goes below 0.25 \AA for all the cases, indicating that these conformational states were indeed visited along the trajectory. Since all the relevant conformations are sampled multiple times during

the metadynamics simulations, the entropic contribution due to these conformational states is naturally accounted in our free energy estimates.

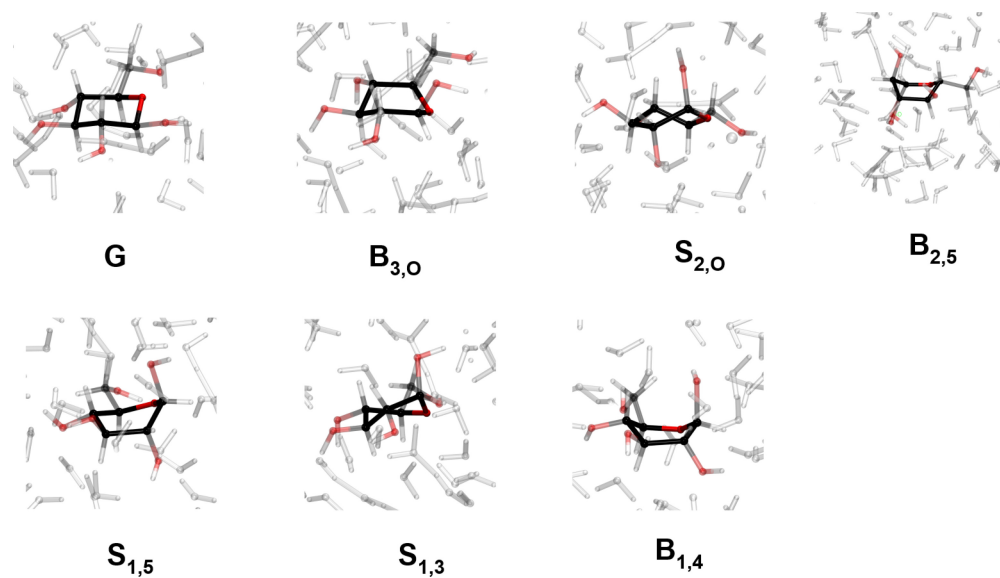


Figure S59: Snapshots of various conformations of **G** sampled during the **G**→**G3** metadynamics simulation. Color codes: C (black), O (red), H (white), solvent molecules (grey colored sticks).

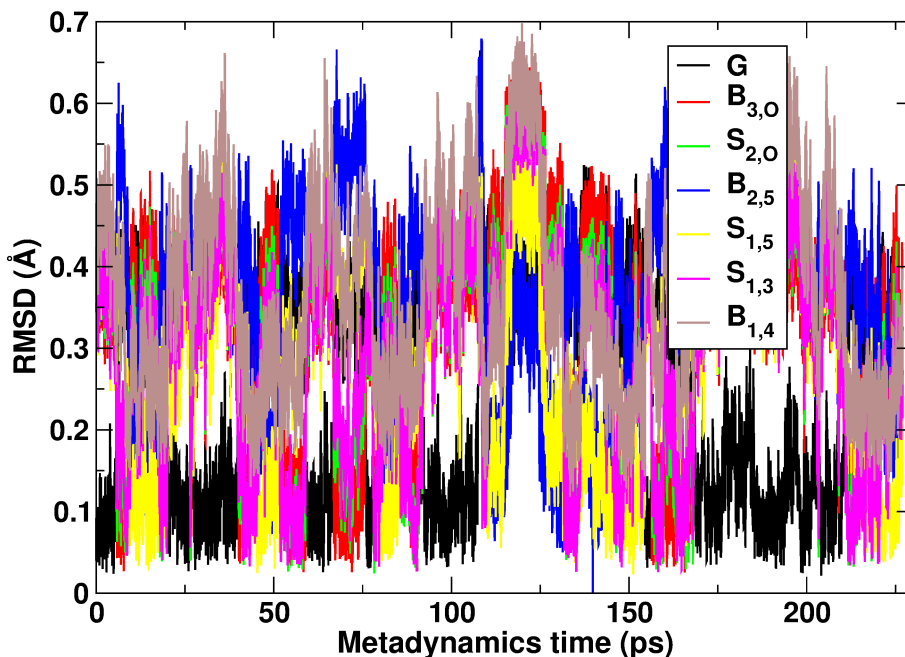


Figure S60: Root mean square deviation (RMSD) (in Å) of the pyranose ring (without the exo-cyclic groups) of **G** in the metadynamics trajectory (ABW conditions) of **G**→**G3** reaction. The RMSD is calculated with respect to the reference conformations of **G** as labeled in Figure S59. The reference structures were gas phase optimized.

9 Analysis of ring opening of **G** (step **G**→**R1**)

The ring opening of **G** to form **R1** was found to occur by the protonation of O5 and deprotonation of O1 through a water chain under both ABW and SCW (Figure S61). The ring opening, proton transfer of O5, and deprotonation of O1 occur simultaneously (Figure S62). Metadynamics simulation shows that during the ring opening process, **G** converts to an open chain structure **R1a** before forming a fully extended open chain of glucose, **R1**. **R1a** differs from **R1** in the distance between O5 and C1. The O5–C1 bond distance was found to be about 3 Å for **R1a**, whereas for **R1** it was found to be about 5 Å (Figure S63).

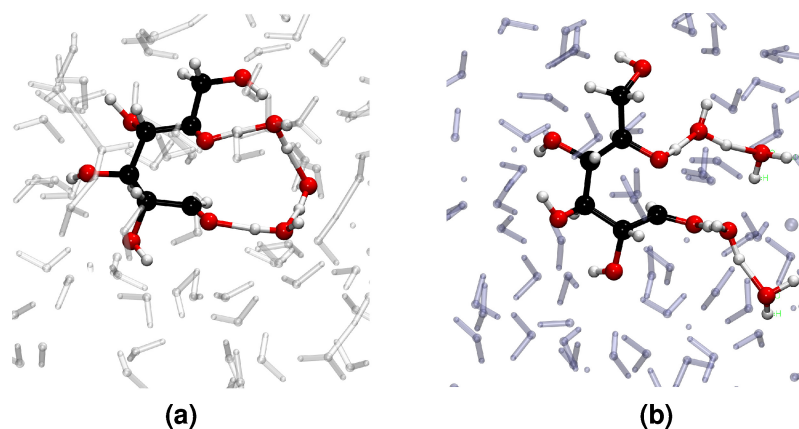


Figure S61: Snapshots of proton transfer during the ring opening of **G** at (a) ABW and (b) SCW conditions. Color codes: C (black), O (red), H (white), solvent molecules (grey colored sticks).

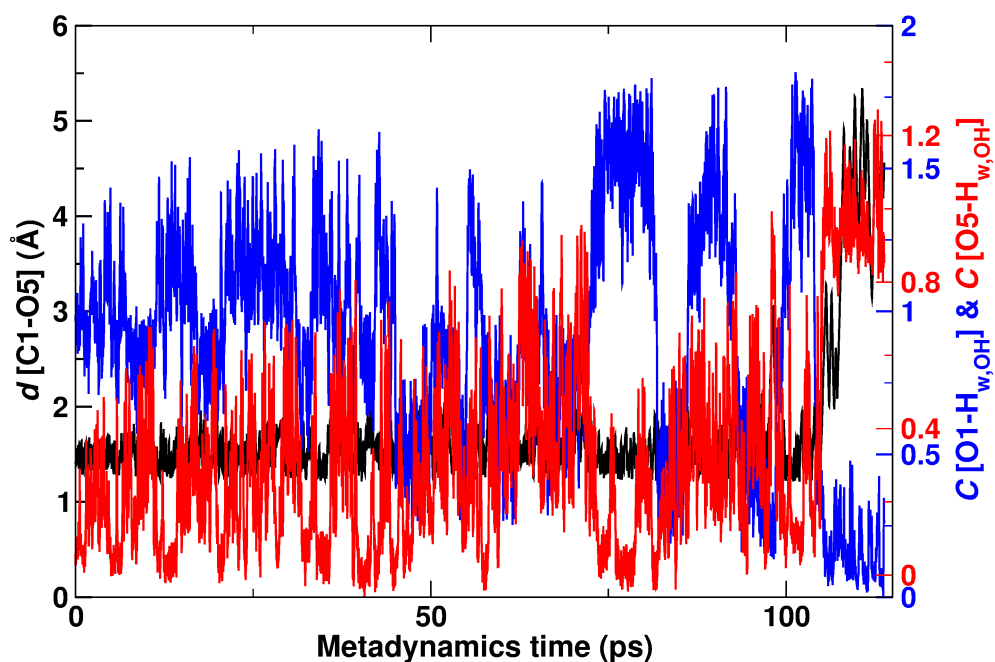


Figure S62: C1-O5 bond distance ($d[\text{C1} - \text{O5}]$) (black; left Y-axis), coordination number between O1 and all the hydrogen atoms of hydroxyl groups as well as water ($C[\text{O1} - \text{H}_{\text{OH,w}}]$) (blue; right Y-axis), and coordination number of O5 with all the hydrogen atoms of hydroxyl groups as well as water ($C[\text{O5} - \text{H}_{\text{OH,w}}]$) (red; right Y-axis) as a function of metadynamics time for the reaction **G**→**R1** under ABW condition.

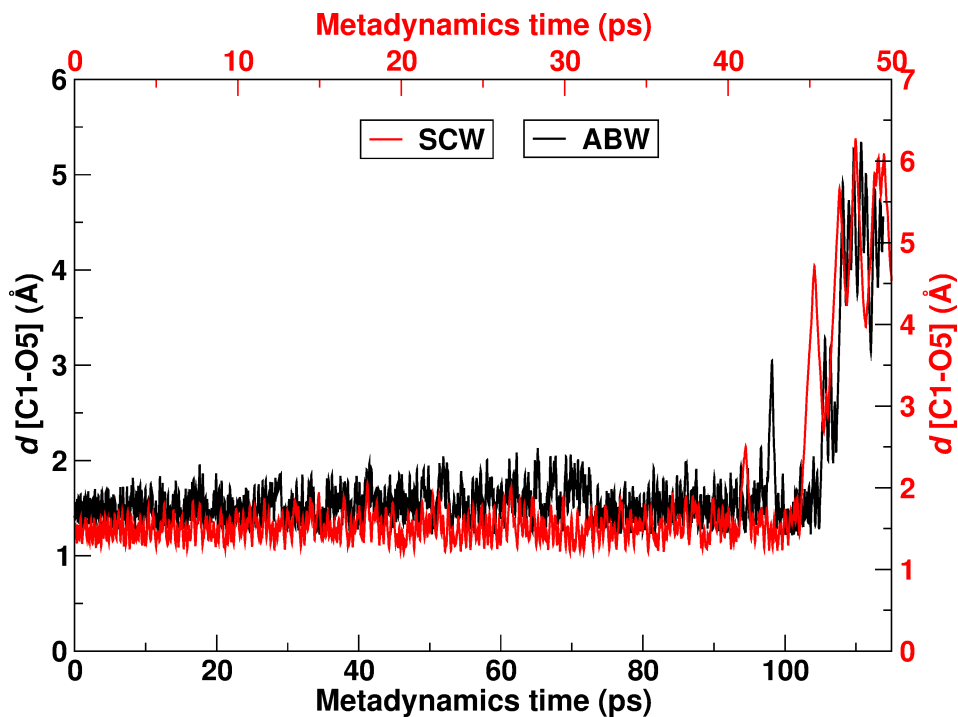


Figure S63: C1-O5 bond distance ($d[\text{C1} - \text{O5}]$) as a function of metadynamics time for the step $\mathbf{G} \rightarrow \mathbf{R1}$ under ABW (black; bottom X-axis and left Y-axis) and SCW (red; top X-axis and right Y-axis).

References

- (1) Perdew, J. P.; Burke, K.; Ernzerhof, M. Generalized Gradient Approximation Made Simple. *Phys. Rev. Lett.* **1996**, *77*, 3865–3868.
- (2) Zhao, Y.; Truhlar, D. G. The M06 Suite of Density Functionals for Main Group Thermochemistry, Thermochemical Kinetics, Noncovalent Interactions, Excited States, and Transition elements: Two New Functionals and Systematic Testing of Four M06-Class Functionals and 12 Other Functionals. *Theoret. Chem. Acc.* **2008**, *120*, 215–241.
- (3) Cossi, M.; Scalmani, G.; Rega, N.; Barone, V. New Developments in the Polarizable Continuum Model for Quantum Mechanical and Classical Calculations on Molecules in Solution. *J. Chem. Phys.* **2002**, *117*, 43–54.

- (4) Bondi, A. van der Waals Volumes and Radii. *J. Phys. Chem.* **1964**, *68*, 441–451.
- (5) Lin, X.; Qu, Y.; Lv, Y.; Xi, Y.; Phillips, D. L.; Liu, C. The First Dehydration and the Competing Reaction Pathways of Glucose Homogeneously and Heterogeneously Catalyzed by Acids. *Phys. Chem. Chem. Phys.* **2013**, *15*, 2967–2982.
- (6) Gaussian 09, Revision B.01, M. J. Frisch, G. W. Trucks, H. B. Schlegel, G. E. Scuseria, M. A. Robb, J. R. Cheeseman, G. Scalmani, V. Barone, B. Men- nucci, G. A. Petersson, H. Nakatsuji, M. Caricato, X. Li, H. P. Hratchian, A. F. Izmaylov, J. Bloino, G. Zheng, J. L. Sonnenberg, M. Hada, M. Ehara, K. Toyota, R. Fukuda, J. Hasegawa, M. Ishida, T. Nakajima, Y. Honda, O. Kitao, H. Nakai, T. Vreven, J. A. Montgomery, Jr., J. E. Peralta, F. Ogliaro, M. Bearpark, J. J. Heyd, E. Brothers, K. N. Kudin, V. N. Staroverov, T. Keith, R. Kobayashi, J. Normand, K. Raghavachari, A. Rendell, J. C. Burant, S. S. Iyengar, J. Tomasi, M. Cossi, N. Rega, J. M. Millam, M. Klene, J. E. Knox, J. B. Cross, V. Bakken, C. Adamo, J. Jaramillo, R. Gomperts, R. E. Strat- mann, O. Yazyev, A. J. Austin, R. Cammi, C. Pomelli, J. W. Ochterski, R. L. Martin, K. Morokuma, V. G. Zakrzewski, G. A. Voth, P. Salvador, J. J. Dan- nenberg, S. Dapprich, A. D. Daniels, O. Farkas, J. B. Foresman, J. V. Ortiz, J. Cioslowski, D. J. Fox, Gaussian, Inc., Wallingford CT., 2010.
- (7) Li, X.; Frisch, M. J. Energy-Represented Direct Inversion in the Iterative Subspace within a Hybrid Geometry Optimization Method. *J. Chem. Theory Comput.* **2006**, *2*, 835–839.
- (8) Biarnés, X.; Ardèvol, A.; Planas, A.; Rovira, C.; Laio, A.; Parrinello, M. The Conformational Free Energy Landscape of β -d-Glucopyranose. Implications for Substrate Preactivation in α -Glucoside Hydrolases. *J. Am. Chem. Soc.* **2007**, *129*, 10686–10693.